Time-Frequency Represetation of Radar Signals Using Doppler-Lag Block Searching Wigner-Ville Distribution

Muhammad Noor Muhammad HAMDI, Ahmad Zuri SHA'AMERI

Department of Electronic and Computer Engineering, School of Electrical Engineering, Universiti Teknologi Malaysia, Johor Bahru, Johor, Malaysia

muhdnoorsel@gmail.com, zuri@fke.utm.my

DOI: 10.15598/aeee.v16i3.2633

Abstract. *Radar signals are time-varying signals where the signal parameters change over time. For these signals, Quadratic Time-Frequency Distribution (QTFD) offers advantages over classical spectrum estimation in terms of frequency and time resolution but it suffers heavily from cross-terms. In generating accurate Time-Frequency Representation (TFR), a kernel function must be able to suppress cross-terms while maintaining auto-terms energy especially in a non-cooperative environment where the parameters of the actual signal are unknown. Thus, a new signal-dependent QTFD is proposed that adaptively estimates the kernel parameters for a wide class of radar signals. The adaptive procedure, Doppler-Lag Block Searching (DLBS) kernel estimation was developed to serve this purpose. Accurate TFRs produced for all simulated radar signals with Instantaneous Frequency (IF) estimation performance are verified using Monte Carlo simulation meeting the requirements of the Cramer-Rao Lower Bound (CRLB) at SNR $>$ 6 dB.*

Keywords

Adaptive procedure, auto-terms, Cramer-Rao lower bound, cross-terms, kernel function, quadratic time-frequency distribution.

1. Introduction

Radar is widely used both in military and non-military applications such as tracking missiles, ships, land vehicles and aircraft, flight control system, ocean surveillance system and geological observations. By definition, Low Probability of Intercept (LPI) radars utilize special emitted waveform that has been specifically designed to avoid detection or interception by non-cooperative intercept receiver [1]. This is achieved by integrating additional properties such as ultra-low sidelobe, Advanced Multifunction Radio Frequency Concept (AMRFC), wideband frequency and minimum transmitted energy. The idea of LPI radar is to see and not be seen, meaning it must have the capability to detect targets like any radar while staying invisible to electronic reconnaissance equipment.

Intercepting LPI signals is not easy but is not totally impossible. Some of the important properties required in the modern intercept receivers in intercepting LPI signals are channelized receiver, utilization of superheterodyne receiver and sidelobe detection capability [2] and [3]. Signal processing algorithms are the important components of modern intercept receiver that improve the detection and analysis of LPI radar signals. Example of methods used for detecting and analyzing LPI radar signals are adaptive match filtering, parallel filter arrays with higher order statistics, Wigner-Ville Distribution (WVD), quadrature mirror filter bank, and cyclostationary processing [3].

A time-varying signal such as LPI radar signals, the spectral description of which depends on time is best analyzed with Time-Frequency Distribution (TFD). Among TFD classes, Quadratic TFD (QTFD) is appropriately used because it provides high-resolution representation both in time and frequency [4]. Cross-terms are introduced in QTFD due to the quadratic nature of the algorithm, which makes it difficult to interpret the true signal characteristics and also exaggerates the effect of noise [5]. Some of the techniques proposed to produce accurate TFR are reduced interference distribution, fractional Fourier transform, Radon-Wigner distribution, adaptive cross WVD and modified B-distribution [6] and [7].

The application of the Fractional Fourier Transform (FrFT) is proven effective in representing and preserving signal components in the Time-Frequency (TF) plane such as Pulse Linear Frequency Modulation (PLFM) [8]. Besides that, the echo of the moving target for airborne Synthetic Aperture Radar (SAR) can also be considered as a LFM signal. Thus, the FrFT can be used to represent and analyze such signals. In the literature, it was mentioned that the FrFT is equivalent to a rotation of the signal either in TF or ambiguity domain. The degree of the TF rotation depends on the fractional power of FrFT [9]. The application of FrFT can be further expanded from this definition for signal parameters estimation and cross-term elimination [10] and [11]. A technique where a combination of a rotated TF plane WVD with a suitable TF filtering is compared with the DLBS-WVD.

The rest of the paper is organized as follows. Section 2. presents the signal model and problem definition. The signal characteristics in the time-lag and Doppler-lag domain are discussed in Sec. 3. The relationship between FrFT and TFR is also explained in this section. The simulation result and discussion are presented in Sec. 4. while the field trials results are described in Sec. 5.

2. Signal Model and Problem Definition

The four commonly used radar signal types utilized to verify the accuracy of time-frequency representation produced by the Doppler-Lag Block Searching Wigner-Ville Distribution (DLBS-WVD) are: Simple Pulse signal (SP), 4 Costas Coded pulse (CC4) signals, PLFM, and Continuous Wave Linear Frequency Modulation (CW-LFM). The signal parameters are described in Tab. 1. Except for the SP signal, all the other signals can be categorized as LPI radar signal waveforms [1]. The signals are assumed that they have been downconverted from radio frequency to intermediate frequency where they are sampled at the Nyquist rate (sampling frequency, $f_s = 40$ MHz).

The use of short pulse repetition period, T between 5 to 20 µs is to simplify the development of the kernel estimation procedure. However, the actual radar signals parameters may vary according to the applications and the detection range [12], [13] and [14].

Typically, Electronic Support (ES) deals with a non-cooperative environment where prior knowledge of the true signal characteristics – pulse repetition period, frequency agilities, modulation techniques, pulse width, pulse amplitude – are unknown. Adaptive kernel improves the TFR by estimating the kernel parameters according to the pattern of cross-terms which vary according to the signal. The QTFD with the adaptive kernel ensures an accurate TFR for a broad class of signals.

Tab. 1: Signal Parameters. Pulse repetition period (T), pulse width (T_p), lowest frequency ($f_{\min}$), highest frequency ($f_{\max}$), bandwidth (BW).

Signal	Frequency Parameters	Time Parameters
Simple Pulse (SP)	$f = 10$ MHz	$T = 5$ µs $T_p = 1$ µs
4 Costas Coded pulse (CC4)	4 sub-pulse frequencies $f_{b1} = 4$ MHz $f_{b2} = 8$ MHz f_{b3}=16 MHz $f_{b4} = 12$ MHz	$T = 16$ µs $T_p = 4$ µs
Pulse Linear FM (PLFM)	$f_{\min} = 2$ MHz $f_{\max} = 17$ MHz $BW = 15$ MHz	$T = 9$ µs $T_p = 4$ µs
Continuous Wave Linear FM (CW-LFM)	$f_{\min} = 2$ MHz $f_{\max} = 10$ MHz $BW = 8$ MHz	$T = 20$ µs $T_p = 10$ µs

3. Quadratic Time-Frequency Distribution

The QTFD produces an energy representation jointly over the time-frequency plane. It is also considered as a related class of filtered WVDs with a specific time–lag kernel function [15]. When expressed with respect to the time-frequency kernel and the WVD, the QTFD is written as [5]

$$\rho_z(t,f) = \gamma(t,f) \overset{**}{_{t\,f}} W_z(t,f), \tag{1}$$

where $\gamma(t,f)$ is a time-frequency kernel and $W_z(t,f)$ is the WVD. The WVD can be defined as

$$W_z(t,f) = \int_{-\infty}^{\infty} K_z(t,\tau)\, e^{-j2\pi f\tau} \mathrm{d}\tau, \tag{2}$$

where $K_z(t,\tau)$ is the bilinear product or Instantaneous Autocorrelation Function (IAF). The bilinear product can be written as

$$K_z(t,\tau) = z\left(t+\frac{\tau}{2}\right) z^*\left(t-\frac{\tau}{2}\right), \tag{3}$$

where $z(t)$ is the analytical form of the signal.

The formulation of the QTFD with the time-lag kernel is given as

$$\rho_z(t,f) = \int_{-\infty}^{\infty} G(t,\tau)^*_t\, K_z(t,\tau)\, e^{-j2\pi f\tau} \mathrm{d}\tau, \tag{4}$$

where $G(t,\tau)$ is the time-lag kernel.

A separable kernel offers independent control of time-smoothing and frequency-smoothing of TFD which can be defined in time-lag function as

$$G(t,\tau) = g_1(t)\, g_2(\tau), \tag{5}$$

where $g_1(t)$ is the smoothing function in time and $g2(\tau)$ is the smoothing function in lag. By using a separable kernel, the QTFD in Eq. (1) can be described as

$$\rho_z(t,f) = \int_{-\infty}^{\infty} g_1(t)^*_{(t)}\, K_z(t,\tau)\, g_2(\tau)\, e^{-j2\pi f\tau} \mathrm{d}\tau. \tag{6}$$

3.1. General Signal Characteristics in Time-Lag Domain

The IAF defined in Eq. (4) can be viewed as the correlation of signal itself over successive time intervals. Cross-terms are introduced due to the quadratic nature of the IAF which can cause difficulty in the interpretation of the true signal characteristics [16] and [17]. Kernel function as shown in Eq. (4) solved this problem.

Various kernel functions gave rise to a range of different TFDs [6] and [15]. The general IAF definition is produced by multiplying the signal with its conjugate as shown in Eq. (7). Each type of input signal, $z(t)$ results in different IAF definition. For example, two pulses of SP signal produce two auto-terms and two cross-terms while two pulses of CW-LFM produce four auto-terms and twelve cross-terms. The IAF obtained by substituting the signal definition in Tab. 1 into Eq. (4) can be expressed in the following form:

$$\begin{aligned} K_z(t,\tau) &= \left[z_1\left(t+\frac{\tau}{2}\right) + z_2\left(t+\frac{\tau}{2}-T\right)\right]\cdot \\ &\cdot \left[z_1^*\left(t-\frac{\tau}{2}\right) + z_2^*\left(t-\frac{\tau}{2}-T\right)\right] \\ &= \underbrace{K_{z,11}(t,\tau) + K_{z,22}(t-T,\tau)}_{\text{auto-terms}} + \\ &\underbrace{K_{z,12}\left(t-\frac{T}{2},\tau+T\right) + K_{z,21}\left(t-\frac{T}{2},\tau-T\right)}_{\text{cross-terms}}, \end{aligned} \tag{7}$$

where $z_1(t)$ is the first pulse and $z_2(t)$ is the second pulse of the signal. The accuracy of TFR depends on the capability of the algorithm to preserve the auto-terms energy. Cross-terms can be divided into two categories: intra-pulse and inter-pulses. Intra-pulse cross-terms occur as a result of the correlation of signal between the sub-pulse of the signal while inter-pulse cross-terms are the product of the correlation between different pulses of the signal.

Figure 1 shows the time-lag domain of CW-LFM signal and produced by replacing $z_1(t)$ and $z_2(t)$ in Eq. (7)

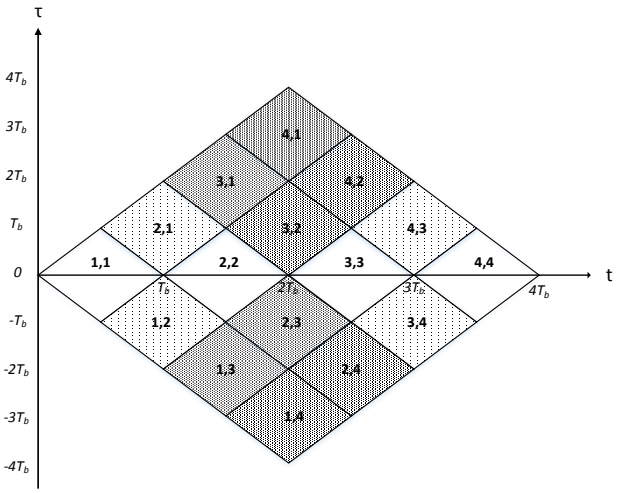

Fig. 1: The time-lag domain two pulses of CW-LFM signal.

with two pulses of triangular CW-LFM signal where T_b is the sub-pulse duration. For triangular CW-LFM, the T_b is exactly half of the signal pulse. The dotted diamond shapes represent the intra-pulse cross-terms and the shaded diamond shapes represent the inter-pulse cross-terms. The remaining diamond shapes represent the auto-terms of the signal.

Generally, a kernel that is able to suppress the cross-terms at $|\tau| > T_b$ is acceptable except for CW-LFM signal. Figure 1 shows that there are some cross-terms located between $0 \leq \tau \leq T_b$ which could lead to inaccurate TFR of the signal. For complete cross-terms suppression, the applied window or kernel must match perfectly with the auto-terms. To completely separate the auto-terms from the cross-terms in the time-lag domain, alternative cross-terms suppression techniques are proposed in the Doppler-lag domain [18].

3.2. Radar Signal Characteristics in Ambiguity Domain

The AF is related to the IAF by the Fourier transform with respect to time as shown in the following equation:

$$A_z(v,\tau) = \underset{t\to v}{FT}\left[K_z(t,\tau)\right] = \int_{-\infty}^{\infty} K_z(t,\tau)\, e^{-j2\pi vt} \mathrm{d}t. \tag{8}$$

The complete signal equations for SP, CC4, PLFM and CW-LFM signals in the ambiguity domain can be found in [19]. The AF for the CW-LFM signal is illustrated in Fig. 2.

The AF represents two pulses CW-LFM signal where the auto-term are represented by the grey shaded shapes, inter-pulse cross-terms by the blue shaded shapes and intra-pulse cross-terms by the orange shaded shapes. Similar color codes are used in Fig. 3,

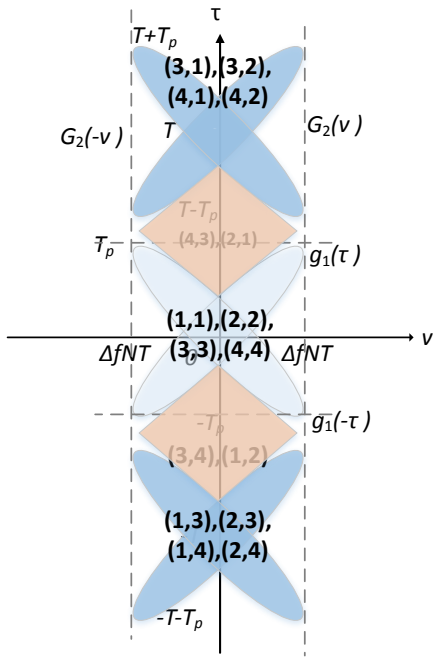

Fig. 2: The AF for two pulses of CW-LFM.

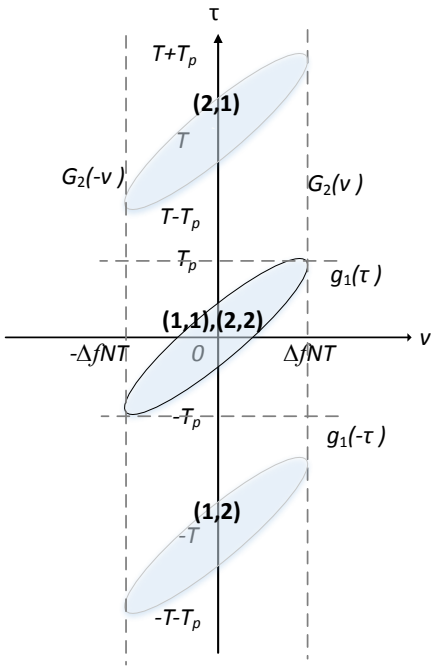

Fig. 3: The AF for two pulses of PLFM signal.

Fig. 4 and Fig. 5. From Fig. 1, the auto-terms are located at $\tau \leq |T_p|$ while most of the intra-pulse cross-terms are positioned very close to the auto-terms. On the other hand, the inter-pulse cross-terms are located between $T - T_p \leq \tau \leq T + T_p$. It is worth mentioning here that the energy of the intra-pulse cross-terms for CW-LFM is significantly lower compared to its auto-terms. Thus, a small portion of the intra-pulse cross-terms in the AF does not cause a major degradation in the TFR.

The procedure for suppressing inter-pulse cross-terms is much simpler in the Doppler-lag domain compared to the time-lag domain because the location between the inter-pulse cross-terms and auto-terms are well separated. Thus, setting a lag window, $g_1(\tau)$ at T_p is sufficient for separating the auto-terms from the inter-pulse cross-terms.

Figure 3 shows the AF for two pulses of PLFM signal. The position of the auto-terms is at $\tau \leq |T_p|$ and the inter-pulse cross-terms are located at $T - T_p \leq \tau \leq T + T_p$. The characteristics of PLFM at the AF are similar with the CW-LFM except there are no intra-pulse cross-terms for PLFM signal. Due to this, the same cross-terms suppression procedure in CW-LFM signal is applicable for PLFM signal.

Figure 4 shows the AF for two pulses of SP signal. Note that the auto-term and inter-pulse cross-terms location are similar with the PLFM and CW-LFM signals which are at $\tau \leq |T_p|$ and $T - T_p \leq \tau \leq T + T_p$ respectively. The only difference is the shape of the auto-terms and the cross-terms. Thus, a similar procedure to attenuate the cross-terms of the PLFM signal can be applied to the SP signal.

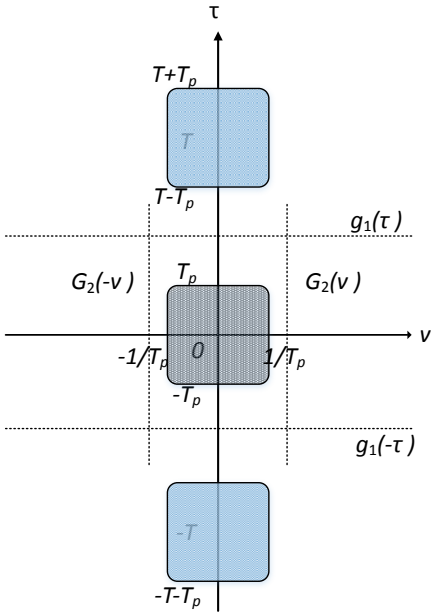

Fig. 4: The AF for two pulses of SP signal.

The AF for one pulse of the CC4 signal is shown in Fig. 5 where the auto-terms of the signal are located at $\tau \leq |T_b|$ while the intra-pulse cross-terms are scattered on the ambiguity plane at $-4T_b \leq \tau \leq 4T_b$. Setting a lag window at $\tau \leq |T_b|$ is enough to extract the auto-terms from the cross-terms in the ambiguity domain.

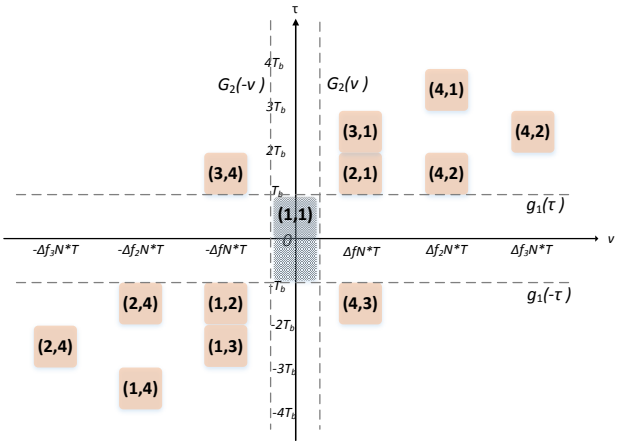

Fig. 5: The AF for one pulse of the CC4 signal.

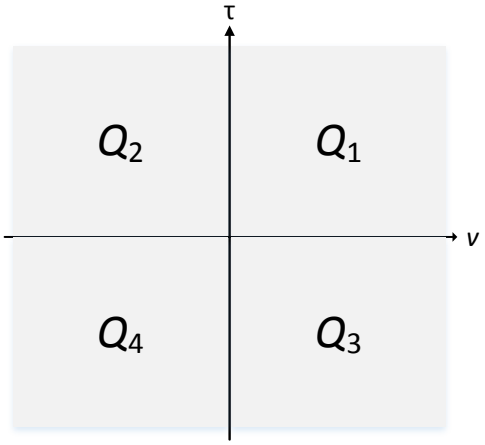

Fig. 6: The quadrant division in the ambiguity domain.

3.3. Estimation of Kernel Parameters

Many studies were conducted to estimate the suitable kernel parameters for reducing the interference in the TFR. Adaptive optimal kernel TFR (AOK-TFR) [20] is one of the earliest techniques that incorporates window in the AF and is able to produce accurate TFR even at SNR of 0 dB. However, the capability of the method is limited to multi-component LFM signals.

Adaptive Optimal Kernel Smooth-Windowed Wigner-Ville Distribution (AOK-SWWVD) [17] and Adaptive Smoothed Windowed cross WVD (ASW-WVD) [15] are also able to produce accurate TFR at a low SNR but these solutions are limited to digitally modulated signals such as FSK and PSK signals. All the methods mentioned above despite proven reliable for signal representation, they lacked the capability to cover a broader class of signals. Thus, the Doppler-Lag Block Searching (DLBS) procedure is introduced in this section to produce an accurate TFR at low SNR while covering a wide class of signals.

Before describing the adaptive procedures, it is crucial to first discuss the four ambiguity function quadrants as shown in Fig. 6. In the DLBS approach, it is sufficient to estimate the kernel parameters only in the Q_1 quadrant due to the symmetrical properties of the ambiguity domain. One of the AF properties exploited is the maximum energy that occurs at the origin of the ambiguity domain.

As defined in [21], the AF is highest at the origin in comparison to the other parts of the ambiguity domain according to the following inequality:

$$|A_z(v,\tau)| \leq |A_z(0,0)|. \tag{9}$$

Thus, the DLBS initiates the search at the origin and checks for a significant drop in energy in Doppler and lag. This is performed by matching the reference block, $A_z(0,0)$ and the analyzed blocks, $A_z(\lambda_1,\lambda_2)$ in the AF domain to obtain the kernel parameters.

The DLBS algorithm can be expressed as follows:

$$\Delta A_z = |A_z(0,0) - A_z(\lambda_1,\lambda_2)|, \tag{10}$$

where ΔA_z is the energy difference between $A_z(0,0)$ and $A_z(\lambda_1,\lambda_2)$ which can be defined as

$$A_z(0,0) = \int_{-\infty}^{\infty}\int_{-\infty}^{\infty} w_a(v,\tau)\, A_z(v,\tau)\, \mathrm{d}v\mathrm{d}\tau.$$

$$A_z(\lambda_1,\lambda_2) = \int_{-\infty}^{\infty}\int_{-\infty}^{\infty} w_a(v-\lambda_1,\tau-\lambda_2)\, A_z(v,\tau)\, \mathrm{d}v\mathrm{d}\tau, \tag{11}$$

$$0 \leq \lambda_1 < \infty, \quad 0 \leq \lambda_2 < \infty,$$

where $w_a(v,\tau)$ is the analysis window, λ_1 is the instant Doppler and λ_2 is the instant lag. The analysis window can be described as [16]

$$w_a(v,\tau) = \frac{v_a}{\tau_a}, \tag{12}$$

$$0 \leq v \leq v_a < \frac{1}{T_p}, \quad 0 \leq \tau \leq \tau_a < T_p,$$

where τ_a and v_a are the analysis window size in terms of lag and Doppler respectively, T_p is the signal pulse width. In order for DLBS to accurately estimate the signal pulse width, the analysis window must be set smaller than the expected signal pulse width.

All the analyzed blocks that have energy difference, Δ_z above the threshold value, $A_{z,thd}$ are considered as a block with a minimum number of auto-terms and can be excluded from the generation of the TFR. Figure 7 shows the Q_1 quadrant for PLFM signal and used as an example for DLBS procedure. The DLBS search procedures are as follows:

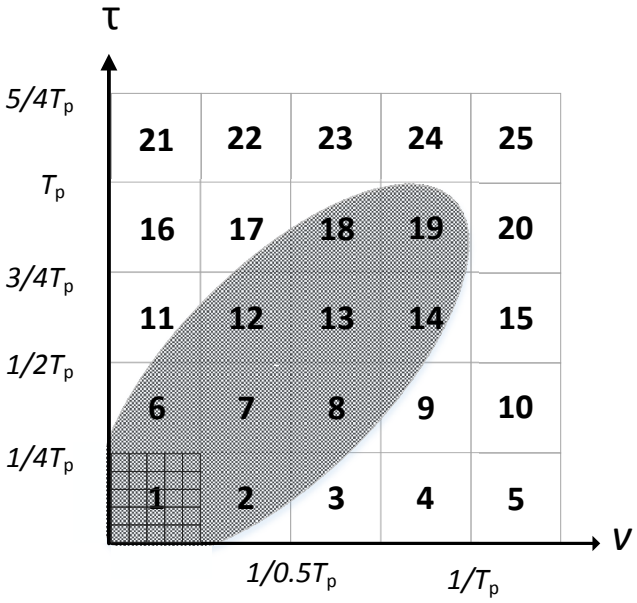

Fig. 7: The Q1 of PLFM in DLBS method.

- Form the Doppler-lag function, $A_z(v,\tau)$ for the Q_1 quadrant using Eq. (8).
- Compute the total energy for block 1 as a reference block, $A_z(0,0)$ and set a threshold value, $A_{z,thd}$.
- Compute the energy difference for block 2, $A_z(1/0.5T_p, 1/4T_p)$. Since the energy difference is below the threshold value continue to the next block on the right.
- The energy difference for block 3, $A_z(1/0.75T_p, 1/4T_p)$ is found to be above the threshold value which means at this particular block the auto-terms energy is low. Hence, the evaluation for row $(1/4)T_p$ is stopped and the evaluation moves to the next row, $(1/2)T_p$.
- The evaluation for new row always starts at one column before the last evaluated column because it will ensure the evaluation start where the auto-terms energy is higher. At the row $(1/2)T_p$ the evaluation starts at block 7.
- The evaluation for row $(1/2)T_p$ starts from block 7 to the right direction until it reaches block 9. Since the energy difference for block 9 is above the threshold value, the search block moves to the next row, $(3/4)T_p$ and start at block 13.
- Steps from 3 to 5 are repeated for the other rows until reached row $(5/4)T_p$. The energy difference for all the blocks in this row are found to be above the threshold value and indicate that the evaluation for PLFM signal is completed.
- The kernel parameter is estimated by choosing the location of last evaluated block that has energy difference below the threshold value. For this example, the last evaluated block is block 19 and its location represent the Doppler and lag parameters which is $1/T_p$ and T_p respectively.

The same procedure is applicable for the other signals as their properties in the AF are similar with the PLFM signal. The threshold value of 0.3 is chosen because it provides the best Doppler and lag window width for most of the signal [19].

3.4. Fractional Fourier Transform in Cross-Terms Reduction

The FrFT is actually a generalized form of Fourier Transform (FT) with the α-th order of fractional power [22] and is best expressed with the help of transformation kernel. If $x(t)$ is the signal, then the FrFT of $x(t)$ is given as [9]

$$X_\alpha(u) = \int_{-\infty}^{\infty} x(t)\, K_\alpha(t,u)\, \mathrm{d}t, \tag{13}$$

where $K_\alpha(t,u)$ is the transformation kernel and can be expressed as

$$K_\alpha(t,u) = \sqrt{\frac{1-j\cot\alpha}{2\pi}}\exp\left(j\frac{t^2+u^2}{2}\cot\alpha - tu\csc\alpha\right). \tag{14}$$

Equation (14) is valid if α is not multiple of π. However, if α is a multiple of 2π, the kernel becomes $\delta(t-u)$. For $(\alpha+\pi)$ a multiple of 2π, the kernel becomes $\delta(t+u)$. The extension of the FrFT to the TFR of the signal is the rotated version of the WVD of the original signal by the angle θ which is given as

$$\rho_{x_\alpha}(t,f) = R_{-\theta}\left\{\rho_x(t,f)\right\}, \tag{15}$$

where $R_\theta\{\}$ is the operator which rotates the TF plane clockwise. If the time-varying signal is linearly separable in the time-frequency plane, the cross-terms can be separated with the appropriate rotation angle and suitable TF filtering technique [5].

3.5. IF Estimate

Instantaneous Frequency (IF) estimation can be used to describe the frequency characteristics of the signal. Normally, a good estimator has to be consistent while statistically and computationally efficient [23]. Rao and Taylor proved that WVD peak based IF estimation is optimal for linear FM signals for moderate and high SNR although the estimator performance degrades significantly at low SNR [24]. Peak based IF estimator can be expressed as

$$\arg\left[\max_f \rho(t,f)\right], \tag{16}$$

where $f_i(t)$ is the IF and $\rho(t, f)$ is the TFR. Peak based IF estimator is able to produce a decent estimation as its capability to localize energy along the IF law [23]. For the purpose of measuring the performance of any unbiased parameter estimator, the Cramer–Rao Lower Bound (CRLB) is frequently used because it can provide the theoretical limit to the variance of the estimator. The most efficient estimator is the one that can achieve the lower bound on the variance [25].

The general formulation of CRLB for IF estimate is [15]

$$\text{var}\left(\hat{f}_l\right) \geq \frac{24}{(2\pi)^2 \gamma N \left(N^2-1\right)}, \tag{17}$$

where N is the average window width, and γ is the SNR. With the assumption that the actual IF of the signal is known, and the signal is in discrete form, the variance of the IF estimated from measurement can be expressed as [15]

$$\text{var}\left(\hat{f}_i\right) = \frac{1}{N}\sum_{n=0}^{N-1}\left(\hat{f}_i(n) - f_i(n)\right)^2, \tag{18}$$

where N is the total number of samples, $\hat{f}_i(n)$ is the actual IF and $f_i(n)$ is the actual IF.

4. Results and Discussion

This section describes the TFRs and IF estimates for SP, CC4, LFM and CW-LFM signals using the DLBS-WVD and FrFT followed by the performance of the IF estimator benchmarked with the CRLB. The performance of DLBS-WVD is presented at SNR of 5 dB. This value is chosen because SNR above 10 dB is considered as high SNR from previous work on IF estimation [15].

4.1. TFR and IF Estimate Performance

By using the DLBS-WVD, the TFR plot and IF estimate for the signals using the parameters presented in Tab. 1 is produced. The energy of auto-terms components is highest at the origin and decrease positioned away from the origin. Due to this, DLBS-WVD has a difficulty to preserve the entire energy of the signal components especially when the auto-terms are located far from the origin. This problem becomes obvious for PLFM and CW-LFM signals compared to SP and CC4 signals as discussed in [19]. A small portion of the auto-terms components are suppressed for PLFM and CW-LFM signals which produced minor errors in the TFR and IF estimate.

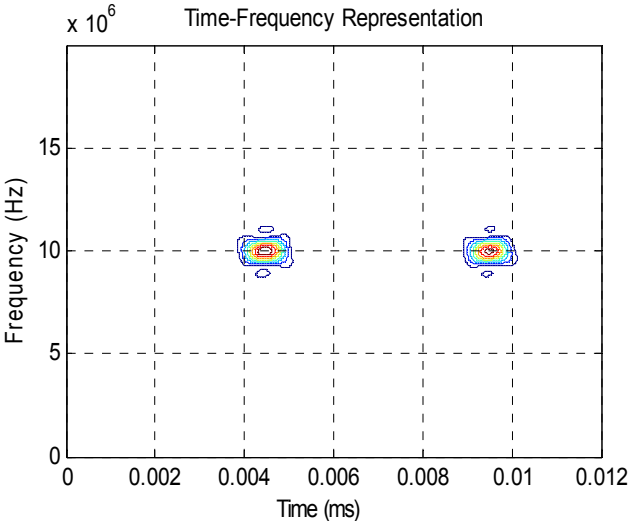

(a) TFR using DLBS.

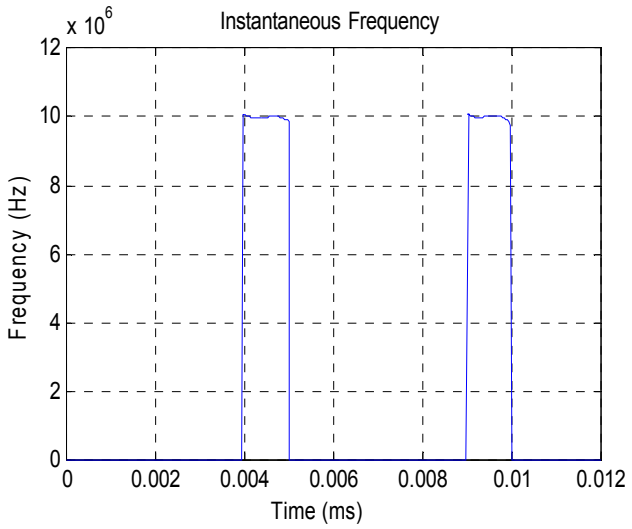

(b) IF using DLBS.

Fig. 8: TFR plot and IF estimate for two pulses SP signal.

Figure 8 shows the TFR plot and IF estimate for a two pulses SP signal. The IF of the signal is accurately estimated at 10 MHz. This is contributed from a clean TFR of the signal due to the successful suppression of the cross-terms in the AF domain.

The TFR and IF estimate for a two pulses CC4 signal is shown in Fig. 9. The frequency components of the signal are correctly estimated given that the Costas sequence of the signal is [1 2 4 3]. In this paper, the CC4 signal is used to illustrate the functionality of the DLBS-WVD on the Costas coded class of signals.

Figure 10 shows the analysis results for a two pulses PLFM signal. The frequency component of the signal is estimated from 2.27–16.75 MHz while T and T_p are 13 ms and 4 ms respectively. The time components of the signal are accurately estimated but the frequency component of the signal is estimated with 1.6 % er-

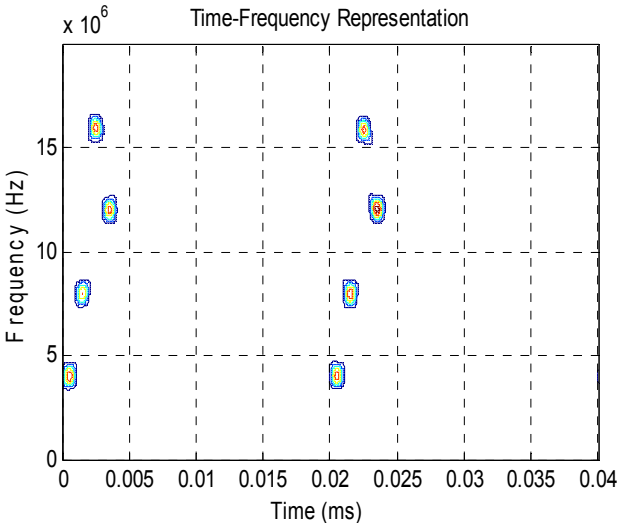

(a) TFR using DLBS.

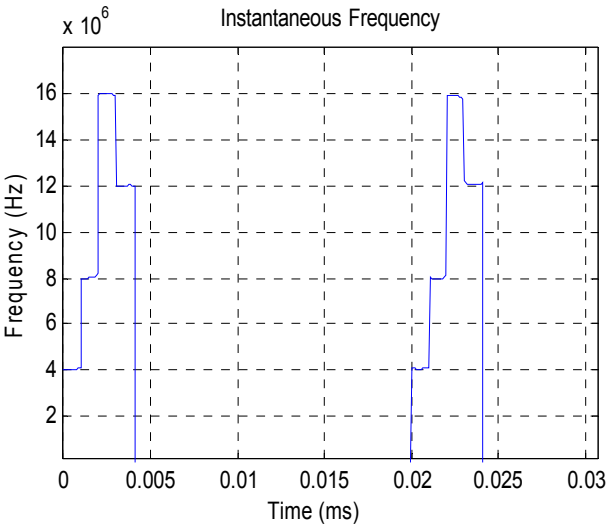

(b) IF using DLBS.

Fig. 9: TFR plot and IF estimate for two pulses CC4 signal.

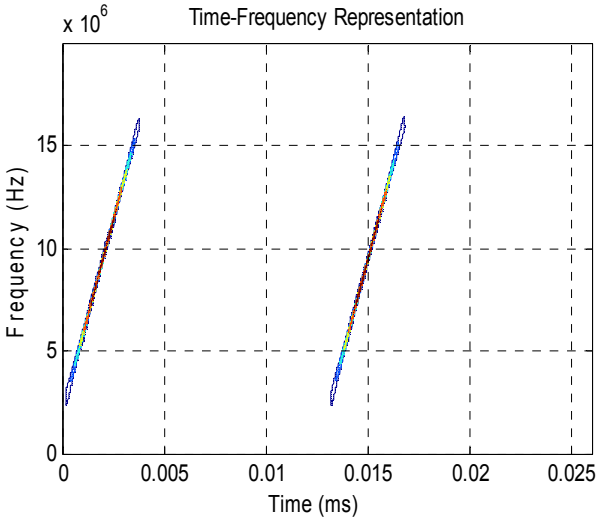

(a) TFR using DLBS.

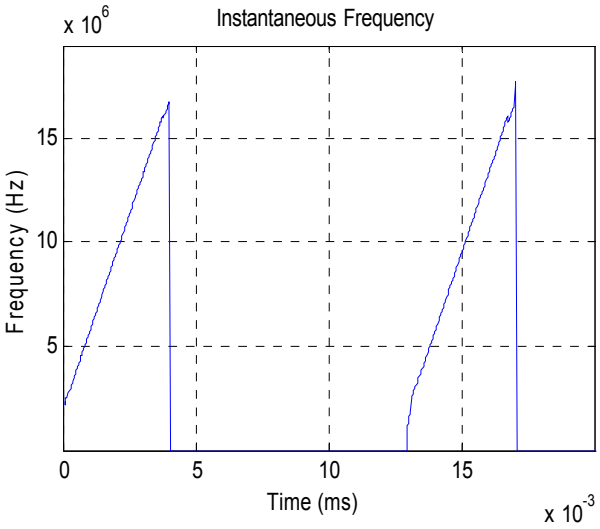

(b) IF using DLBS.

Fig. 10: TFR plot and IF estimate for two pulses PLFM signal.

ror. This error is due to inevitable suppression of the small part of signal auto-terms in the ambiguity domain. However, the estimation error is too small and can be considered insignificant.

The TFR and IF estimate is shown in Fig. 11 for a two pulses CW-LFM signal. The minimum and maximum frequency of the signal is estimated at 2.19 MHz and 5.83 MHz respectively. There is about 4.2 % error in the frequency component estimation which is slightly higher than the LFM signal. This is due to the intra-pulse cross-terms in the CW-LFM signal which reduces the energy concentration of the signal components and produce errors in the IF estimation.

4.2. TFR of WVD Using FrFT

Using the same signal as in the previous section, the performance of FrFT in producing an accurate TFR is evaluated. The IF estimate of the signal using FrFT is similar to the result from the previous section given that the cross-terms are successfully removed. It is important to perform a TF rotation in such a way that the fractional frequency spectrum is most compact before applying any TF filtering procedure. The technique used in determining the correct order of FrFT is searching scheme [26]. This method determines the optimal fractional power by evaluating the compactness of the fractional frequency spectrum. The fractional power that provides the most compact fractional spectrum will be used for TF filtering.

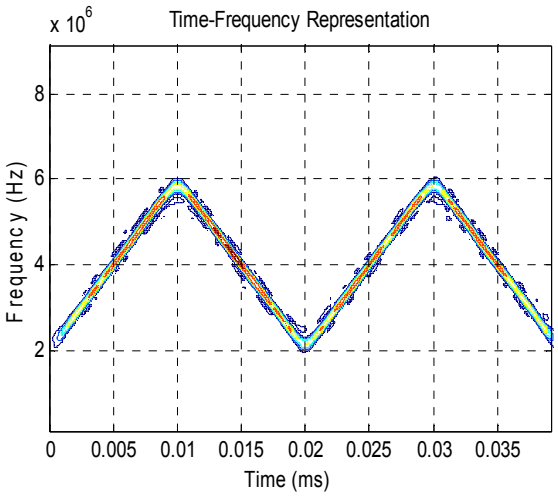

(a) TFR using DLBS.

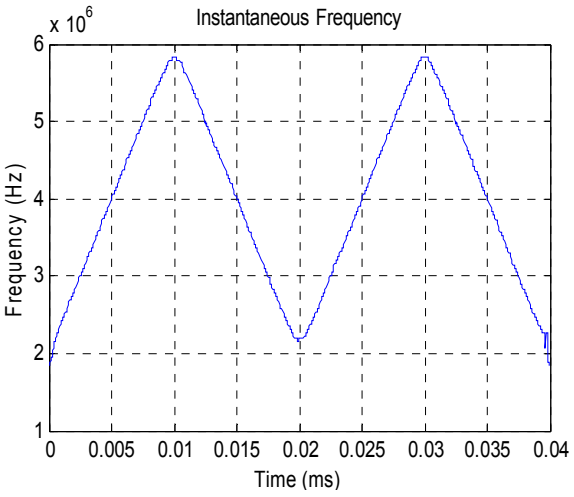

(b) IF using DLBS.

Fig. 11: TFR plot and IF estimate for two pulses CW-LFM signal.

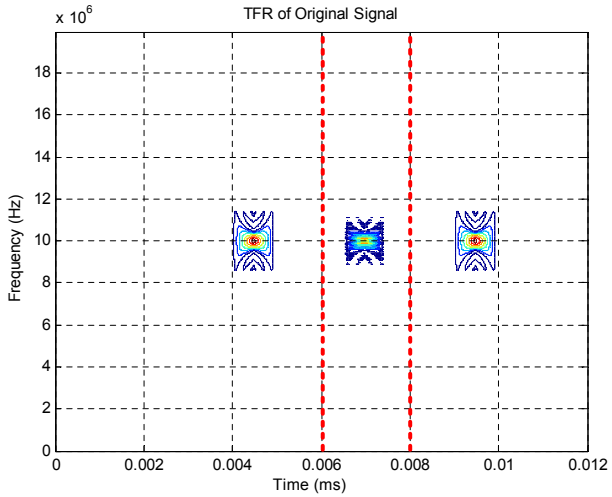

(a)

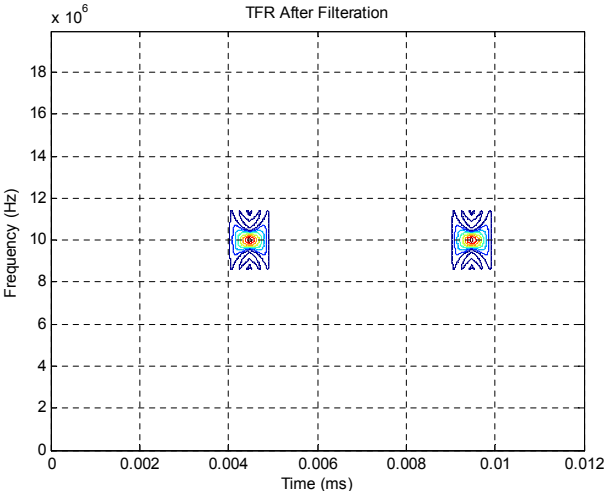

(b)

Fig. 12: TFR plot for two pulses SP signal.

The SP signal does not require any TF rotation since the frequency spectrum is most compact at fractional power zero. The cross-terms that are located between the signal components can be easily removed by applying a TF filtering as shown in Fig. 12(a) with a red dotted line resulting in as shown in Fig. 12(b) a cross-terms free TFR of the SP signal.

Figure 13 shows a TFR plot for two pulses of CC4 signal which is heavily corrupted by cross-terms. For every pulse of CC4 signal, there are four signal components representing four different frequencies as indicated by red dotted boxes. The localization of cross-terms that are very close to the auto-terms result in strong degradation of signal power. There is no suitable rotation angle that can be used to completely remove all the cross-terms. Furthermore, the smearing effect from the cross-terms further reduce the quality of the signal components especially at a frequency of

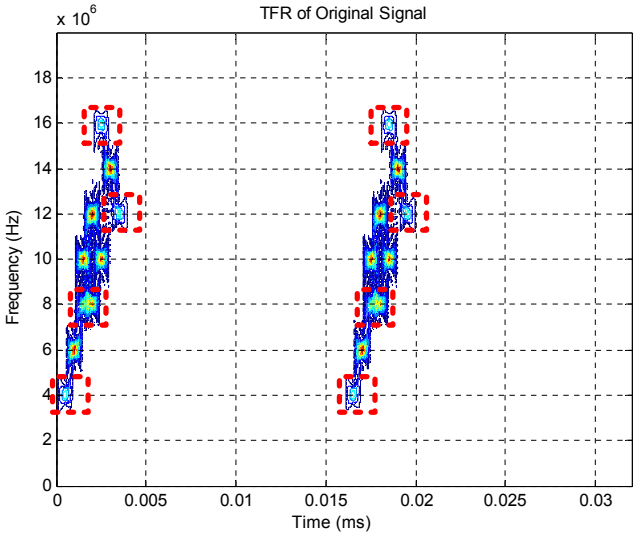

Fig. 13: TFR plot for two pulses CC4 signal.

8 MHz. In short, the combination of FrFT and TF filtering is insufficient to provide accurate TFR for CC4 signal.

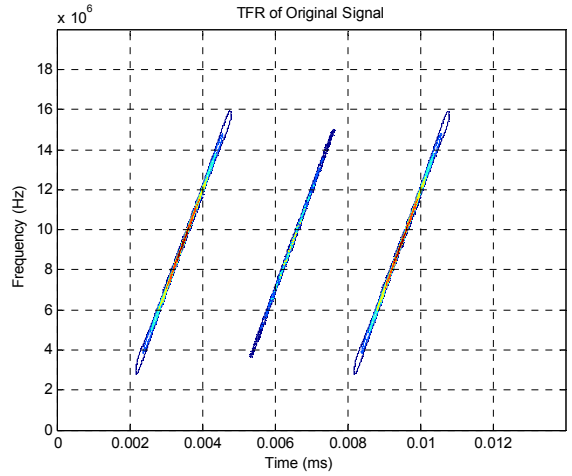

(a)

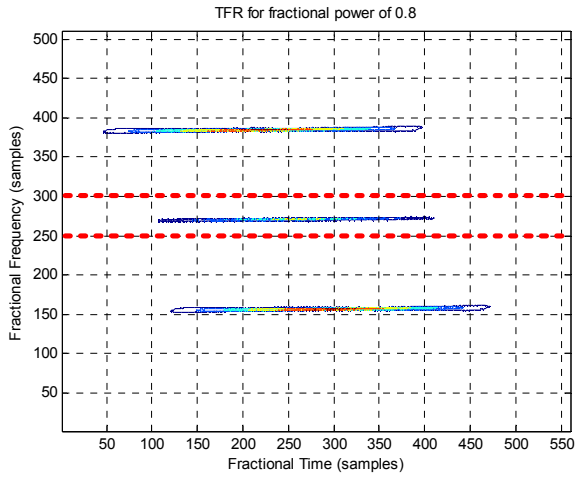

(b)

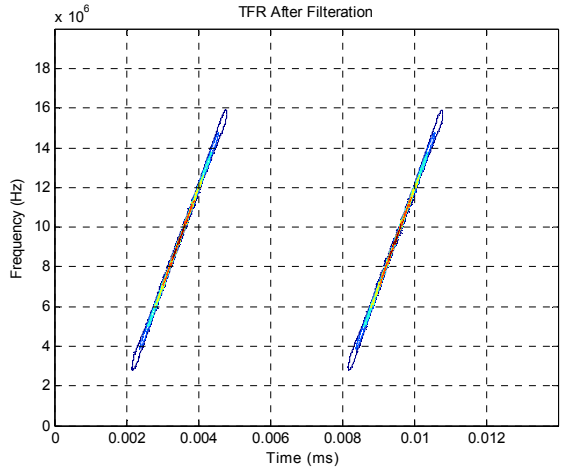

(c)

Fig. 14: TFR plot for two pulses CW-LFM.

Figure 14(a) shows a PLFM signal that is corrupted with cross-terms. The first step in preserving the signal components is by rotating the TF plane until the fractional frequency spectrum achieved the highest compactness. In this case, the highest compactness is obtained at the fractional power of 0.8 as shown in Fig. 14(a). The next step is to apply a TF filter between the fractional frequency of 250 and 300 in samples. By applying a filter at this location, the entire cross-terms can be completely removed as described in Fig. 14(b).

Next, a reverse TF rotation with the fractional power of -0.8 needs to be performed to obtain an actual representation of signal since the current representation is in the fractional domain. The resulting cross-term free representation after the TF filter is applied for the PLFM signal is shown in Fig. 14(c).

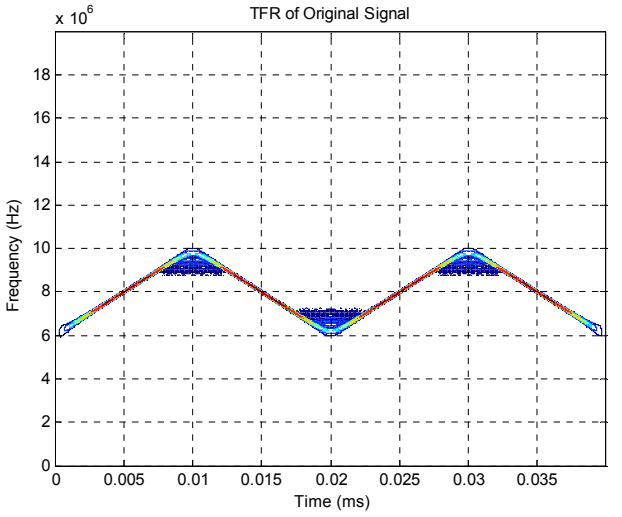

(a)

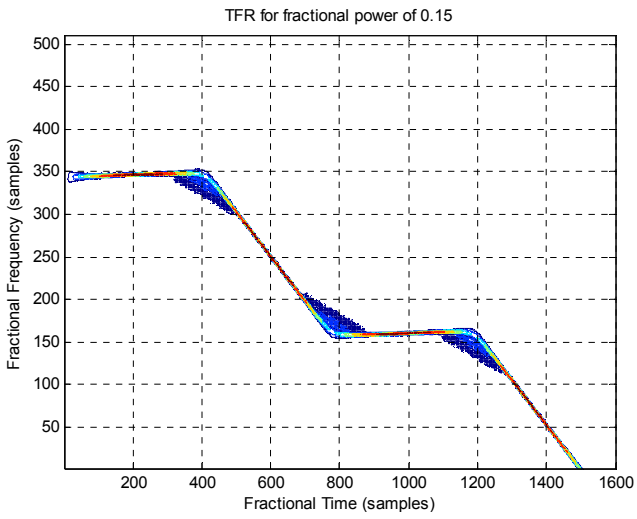

(b)

Fig. 15: TFR plot for two pulses CW-LFM.

The TFR for the CW-LFM signal is shown in Fig. 15. The cross-terms are located between the positive chirp and negative chirp of the signal. Removing the cross-terms for CW-LFM signal appear to be difficult. For example, at a fractional power of 0.15, if a TF filter is placed around samples of 350 the first positive chirp of the signal could be extracted but with the cost of removing the rest of the signal. The effect of the cross-terms is more noticeable at lower SNR because the energy of the signal components is much lower.

As a conclusion, it is shown in this section that the combination of FrFT and TF filtering could only produce accurate TFR for SP and PLFM signals. The DLBS-WVD is able to cover a wide class of signal including CW-LFM and CC4 signals. Besides that, in the DLBS-WVD there is no requirement for finding the correct rotation angle of the TF plane before filtering which translates as reduced computational cost.

4.3. IF Estimate Variance Comparison

The IF estimate variance is used to evaluate the performance of the DLBS-WVD in the presence of noise. Monte Carlo simulations based on 100 realizations for SNR range from -7 dB to 17 dB were performed to verify the performance of the DLBS-WVD at both low and high SNRs. Figure 16, Fig. 17, Fig. 18 and Fig. 19 show the IF estimate variance for SP, CC4, PLFM and CW-LFM signals at SNR range from -7 dB to 16 dB.

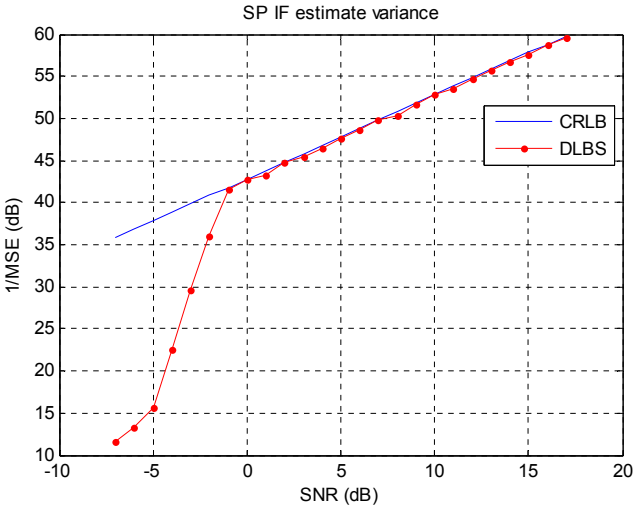

Fig. 16: IF estimate variance comparison for SP signal.

For the SP signal, the IF estimate variance meets the CRLB down to the cut-off SNR ≥ -1 dB. Similar results are also obtained for the CC4 and PLFM signals. There is a significant drop in the IF estimate variance in the CRLB below the cut-off SNR due to the fact that the cross-terms energy is relatively higher compared to the auto-terms energy. For CW-LFM signal, the cut-off SNR is at 4 dB as shown in Fig. 19. The slight increase in the cut-off SNR in CW-LFM signal

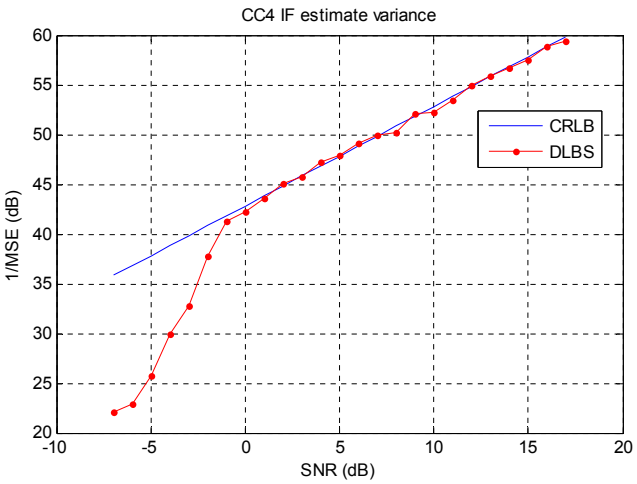

Fig. 17: IF estimate variance comparison for the CC4 signal.

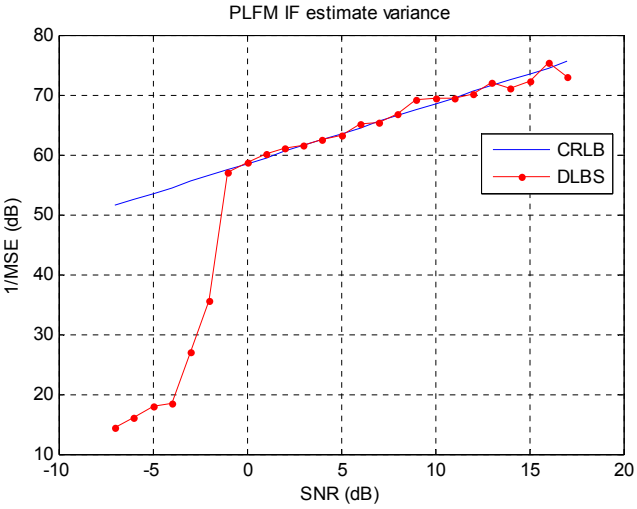

Fig. 18: IF estimate variance comparison for PLFM signal.

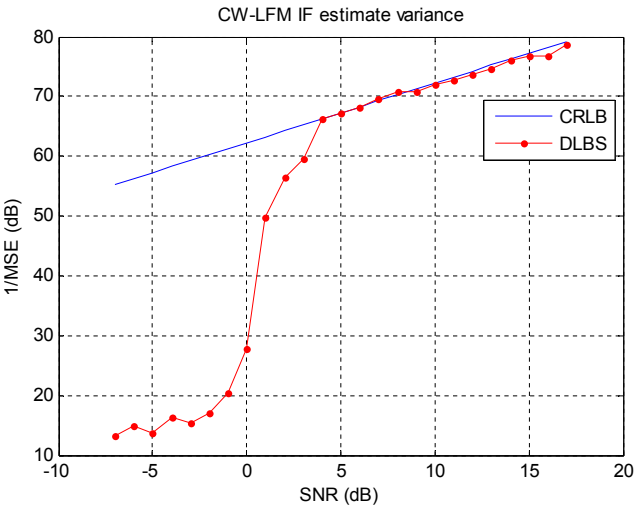

Fig. 19: IF estimate variance comparison for CW-LFM signal.

because the intra-pulse cross-terms in the ambiguity domain reduce the effectiveness of DLBS-WVD in estimating accurate kernel parameters.

5. Field Trials

To validate the DLBS-WVD in a practical environment, an actual radar signal is captured and analyzed. The signal was captured from an interrogator of the Secondary Surveillance (SSR) at the Senai International Airport, Johor Bahru, Malaysia, in August 2016. An Ettus N210 Software Defined Radio (SDR) was used to capture the signal and detail analysis was conducted in Matlab software.

The signal at a carrier frequency of 1030 MHz was then down-converted to an intermediate frequency of 2 MHz. A sampling frequency of 20 MHz was used to convert the intermediate frequency signal to discrete-time for analysis in Matlab. Figure 20 shows the time representation of the signal and the pulse repetition period is estimated at 3.6 ms.

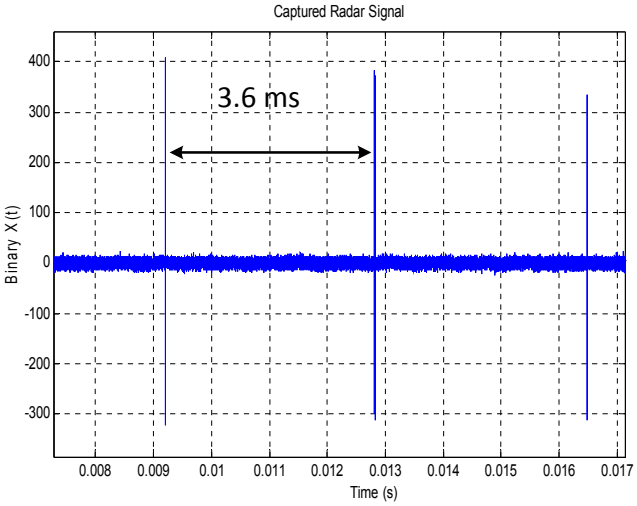

Fig. 20: The time representation of the captured radar signal.

The TFR for one pulse of the signal is shown in Fig. 21. The signal consists of three sub-pulses where the separation between first and second sub-pulse is 2 µs while the separation between first and third sub-pulse is 21 µs. Based on the estimated time separation, the signal exhibits the characteristics of a Mode C interrogation format [27] with an estimated SNR of about 32.7 dB. Such high energy signal is obtained due to the close proximity between the SSR and the receiving equipment.

Figure 22 shows the IF estimate for one pulse of the captured SSR signal. The estimated frequency of the recorded radar signal is 1.2 MHz. A better TFR and IF estimate of the signal can be obtained by increasing

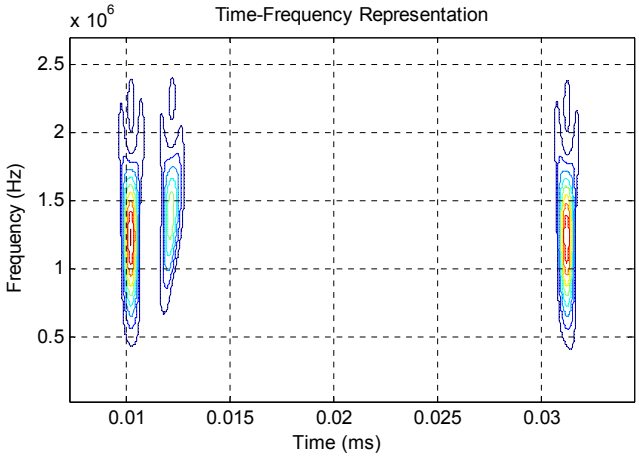

Fig. 21: The TFR for one pulse of the recorded SSR signal.

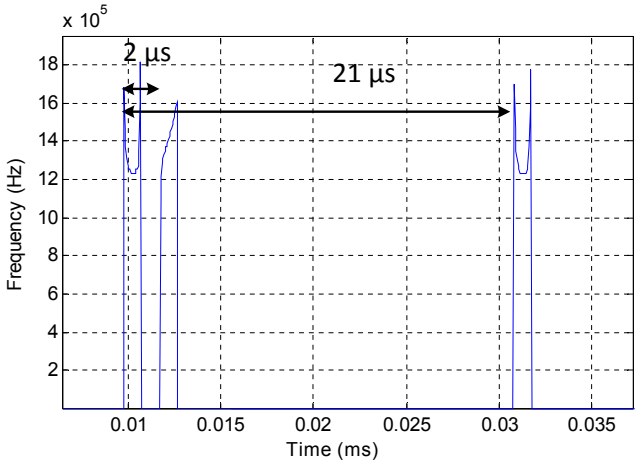

Fig. 22: The IF estimate for one pulse of the captured SSR signal.

the sampling frequency to produce a bigger separation between the auto-terms and the cross-terms in the ambiguity domain.

Although the DLBS-WVD is able to provide accurate time-frequency representation, there is a limitation to the method. The effectiveness and accuracy of DLBS-WVD hold true if the separation between two pulses is greater than the pulse width of the signal.

6. Conclusion

This research accomplished the objective to achieve accurate time-frequency representation of radar signals (SP, CC4, PLFM, and CW-LFM) using the DLBS-WVD. The estimated IF met the CRLB at SNR of −1 dB for SP, CC4, and PLFM signals, and at SNR of 4 dB for CW-LFM signal. In comparison, DLBS-WVD performs better than the combination of FrFT and TF filtering in terms of representing a wide number of signal classes. DLBS-WVD is able to accurately rep-

resent all four signal classes while FrFT is only capable of representing LFM and SP signals. The practicality of the DLBS-WVD was demonstrated using actual signal captured from an SSR radar site. Both time and frequency parameters such as pulse repetition period, pulse width and frequency components were successfully estimated.

Acknowledgment

The authors thank Yayasan Sultan Iskandar for sponsoring this research from the start until the completion of this research. We would also like to show our gratitude to Universiti Teknologi Malaysia (UTM) and Ministry of Higher Education (MOHE) for providing the resources and support for this research.

References

[1] RAVIPRAKASH, G., P. TRIPATHI and B. RAVI. Generation of low probability of intercept signals. *International Journal of Scientific Engineering and Technology*. 2013, vol. 2, iss. 9, pp. 835–839. ISSN 2277-1581.

[2] STOVE, A. G., A. L. HUME and C. J. BAKER. Low probability of intercept radar strategies. *IEE Proceedings - Radar, Sonar and Navigation*. 2004, vol. 151, iss. 5, pp. 249–260. ISSN 1350-2395. DOI: 10.1049/ip-rsn:20041056.

[3] DENK, A. *Detection and jamming low probability of intercept (LPI) radar*. Monterey, 2006. Master thesis. Naval Postgraduate School. Supervisor: Edward Fisher.

[4] GAU, J. *Analysis of low probability of intercept (LPI) radar signals using the Wigner distribution*. Monterey, 2002. Master thesis. Naval Postgraduate School. Supervisor: Phillip E. Pace.

[5] BOASHASH, B. *Time-Frequency Signal Analysis and Processing*. London: Academic Press, 2015. ISBN 978-0123984999.

[6] SEJDIC, E., I. DJUROVIC and J. JIN. Time–frequency feature representation using energy concentration: An overview of recent advances. *Digital Signal Processing*. 2009, vol. 19, iss. 1, pp. 153–183. ISSN 1051-2004. DOI: 10.1016/j.dsp.2007.12.004.

[7] LERGA, J., V. SUCIC and B. BOASHASH. An Efficient Algorithm for Instantaneous Frequency Estimation of Nonstationary Multicomponent Signals in Low SNR. *EURASIP Journal on Advances in Signal Processing*. 2011, vol. 2011, iss. 1, pp. 1–16. ISSN 1687-6180. DOI: 10.1155/2011/725189.

[8] SUN, H.-B., G.-S. LIU and W.-M.-SU. Application of the fractional Fourier transform to moving target detection in airborne SAR. *IEEE Transactions on Aerospace and Electronic Systems*. 2002, vol. 38, iss. 4, pp. 1416–1424. ISSN 0018-9251. DOI: 10.1109/TAES.2002.1145767.

[9] PEI, S.-C. and J.-J. DING. Relations Between Gabor Transforms and Fractional Fourier Transforms and Their Applications for Signal Processing. *IEEE Transactions on Signal Processing*. 2007, vol. 55, iss. 10, pp. 4839–4850. ISSN 1053-587X. DOI: 10.1109/TSP.2007.896271.

[10] KHAN, N. A., I. A. TAJ, M. N. JAFFRI and S. IJAZ. Cross-term elimination in Wigner distribution based on 2D signal processing techniques. *Signal Processing*. 2011, vol. 91, iss. 3, pp. 590–599. ISSN 0165-1684. DOI: 10.1016/j.sigpro.2010.06.004.

[11] QAZI, S., A. GEORGAKIS, L. K. STERGIOULAS and M. SHIKH-BAHAEI. Interference Suppression in the Wigner Distribution Using Fractional Fourier Transformation and Signal Synthesis. *IEEE Transactions on Signal Processing*. 2007, vol. 55, iss. 6, pp. 3150–3154. ISSN 1053-587X. DOI: 10.1109/TSP.2007.893971.

[12] KEERTHI, Y. and T. D. BHATT. LPI radar signal generation and detection. *International Research Journal of Engineering and Technology*. 2015, vol. 2, iss. 7, pp. 721–727. ISSN 2395-0056.

[13] TOUATI, N., C. TATKEU, T. CHONAVEL and A. RIVENQ. Phase Coded Costas Signals for Ambiguity Function Improvement and Grating Lobes Suppression. In: *78th Vehicular Technology Conference*. Las Vegas: IEEE, 2013, pp. 1–5. ISBN 978-1-4673-6187-3. DOI: 10.1109/VTCFall.2013.6692362.

[14] PACE, P. E. *Detecting and Classifying Low Probability of Intercept Radar*. Norwood: Artech House, 2009. ISBN 978-1596932340.

[15] CHEE. Y. *Adaptive Cross Wigner-Ville Distribution For Parameter Estimation Of Digitally Modulated Signals*. Skudai, 2013. Dissertation thesis. Universiti Teknologi Malaysia. Supervisor: Ahmad Zuri Sha'ameri.

[16] CHEE, Y. M, A. Z. SHA'AMERI and M. M. A. ZABIDI. IF estimation of FSK signals using adaptive smoothed windowed cross Wigner–Ville distribution. *Signal Processing*. 2014, vol. 100, iss. 1, pp. 71–84. ISSN 0165-1684. DOI: 10.1016/j.sigpro.2013.12.031.

[17] TAN, J. L. and A. Z. SHA'AMERI. Adaptive optimal kernel smooth-windowed Wigner-Ville distribution for digital communication signal. *EURASIP Journal on Advances in Signal Processing*. 2008, vol. 2008, iss. 1, pp. 1–17. ISSN 1687-6180. DOI: 10.1155/2008/408341.

[18] O'TOOLE, J. M. and B. BOASHASH. Fast and memory-efficient algorithms for computing quadratic time–frequency distributions. *Applied and Computational Harmonic Analysis*. 2013, vol. 35, iss. 2, pp. 350–358. ISSN 1063-5203. DOI: 10.1016/j.acha.2013.01.003.

[19] HAMDI, M. *Adaptive Time-Frequency Distribution for Accurate Representation of Radar Signals*. Skudai, 2017. Master thesis. Universiti Teknologi Malaysia. Supervisor: Ahmad Zuri Sha'ameri.

[20] JONES, D. L. and R. G. BARANIUK. An adaptive optimal-kernel time-frequency representation. *IEEE Transactions on Signal Processing*. 1995, vol. 43 iss. 10, pp. 2361–2371. ISSN 1053-587X. DOI: 10.1109/78.469854.

[21] LEVANON, N. and E. MOZESON. *Radar Signals*. New Jersey: John Wiley & Sons, 2004. ISBN 978-0471473787.

[22] SEJDIC, E., I. DJUROVIC and L. STANKOVIC. Fractional Fourier transform as a signal processing tool: An overview of recent developments. *Signal Processing*. 2011, vol. 91, iss. 6, pp. 1351–1369. ISSN 0165-1684. DOI: 10.1016/j.sigpro.2010.10.008.

[23] BOASHASH, B. Estimating and interpreting the instantaneous frequency of a signal. II. Algorithms and applications. *Proceedings of the IEEE*. 1992, vol. 80, iss. 4, pp. 540–568. ISSN 1558-2256. DOI: 10.1109/5.135378.

[24] RAO, P. and F. J. TAYLOR. Estimation of instantaneous frequency using the discrete Wigner distribution. *Electronics Letters*. 1990, vol. 26, iss. 4, pp. 246–248. ISSN 0013-5194. DOI: 10.1049/el:19900165.

[25] LOVELL, B. C. and R. C. WILLIAMSON. The statistical performance of some instantaneous frequency estimators. *IEEE Transactions on Signal Processing*. 1992, vol. 40, iss. 7, pp. 1708–1723. ISSN 1941-0476. DOI: 10.1109/78.143443.

[26] CAPUS, C. and K. BROWN. Short-time fractional Fourier methods for the time-frequency representation of chirp signals. *The Journal of the Acoustical Society of America*. 2003, vol. 113, iss. 6, pp. 3253–3263. ISSN 1520-8524. DOI: 10.1121/1.1570434.

[27] Radartutorial: Book 2 Radar Sets. *Radartutorial.eu* [online]. 2000. Available at: `http://www.radartutorial.eu/druck/Book2.pdf`.

About Authors

Muhammad Noor Muhammad HAMDI received his B.Eng. degree and M. Eng. in Electrical Engineering both from Universiti Teknologi Malaysia in 2013 and 2017 respectively. He was a student member of Digital Signal and Image Processing (DSIP) Research Group and currently employed as a research assistant. His research interests include signal processing, including time-frequency and time-varying signal analysis especially for radar application, Verilog system design, and microcontroller programming. He also from time to time provides necessary guidance and consultation for bachelor and master degree student in the related field of interest.

Ahmad Zuri SHA'AMERI obtained his B.Sc. in Electrical Engineering from the University of Missouri, Columbia, USA in 1984, and M.Eng. Electrical Engineering and Ph.D. both from UTM in 1991 and 2000 respectively. At present, he is an associate professor, Coordinator for the Digital Signal and Image Processing (DSIP) Research Group and Academic Coordinator for the DSP Lab, Electronic and Computer Engineering Department, Faculty of Electrical Engineering, UTM. His research interest includes signal theory, signal processing for radar and communication, signal analysis and classification, and information security. He has also conducted short courses for both government and private sectors. At present, he has published 160 papers in his areas of interest at both national and international levels in conferences and journals.